Tunable Magnetoacoustic Oscillator with Low Phase Noise

A. Litvinenko,[1,*] R. Khymyn,[2] V. Tyberkevych,[3] V. Tikhonov,[1] A. Slavin,[3] and S. Nikitov[1,4,5]

[1] *Laboratory of Metamaterials, Saratov State University, Saratov 410012, Russia*
[2] *Department of Physics, University of Gothenburg, Gothenburg 412 96, Sweden*
[3] *Department of Physics, Oakland University, Rochester 48309, Michigan, USA*
[4] *Kotelnikov Institute of Radioengineering and Electronics of Russian Academy of Sciences, Moscow 125009, Russia*
[5] *Moscow Institute of Physics and Technology (National Research University), Dolgoprudny 141700, Moscow Region, Russia*

(Received 17 November 2020; revised 2 February 2021; accepted 10 February 2021; published 18 March 2021)

A frequency-tunable low-phase-noise magnetoacoustic resonator is developed on the base of a parallel-plate straight-edge bilayer consisting of an yttrium-iron-garnet (YIG) layer grown on a substrate of a gallium gadolinium garnet (GGG). When a YIG-GGG sample forms an ideal parallel plate, it supports a series of high-quality-factor acoustic modes standing along the plate thickness. Due to the magnetostriction of the YIG layer the ferromagnetic resonance (FMR) mode of the YIG layer can strongly interact with the acoustic thickness modes of the YIG-GGG structure, when the modes' frequencies match. A particular acoustic thickness mode used for the resonance excitations of the hybrid magnetoacoustic oscillations in a YIG-GGG bilayer is chosen by the YIG-layer FMR frequency, which can be tuned by the variation of the external bias magnetic field. A composite scheme of a magnetoacoustic oscillator, which includes a FMR-based resonance preselector, is developed to guarantee satisfaction of the Barkhausen criteria for a single-acoustic-mode oscillation regime. The developed low-phase-noise composite magnetoacoustic oscillator can be tuned from 0.84 to 1 GHz with an increment of about 4.773 MHz (frequency distance between the adjacent acoustic thickness modes in a YIG-GGG parallel plate), and demonstrates the phase noise of −116 dBc/Hz at the offset frequency of 10 kHz.

DOI: 10.1103/PhysRevApplied.15.034057

I. INTRODUCTION

One of the most useful tasks in modern communication and radar technology is the development of reference oscillators with low phase noise, as the low level of phase noise translates into a high level of frequency stability necessary for improved device performance. Also, in digital communication systems, phase noise affects the system bit-error rate, and, therefore, the speed of data processing. In radar applications, lowering the phase noise leads to an increase of radar range and sensitivity, as it allows detections of a signal reflected from the target with a lower power level.

In many common applications, reference or local *tunable* oscillators are based on yttrium-iron-garnet (YIG) resonators, because the frequency of ferromagnetic resonance (FMR) in YIG can be easily tuned over a decade by applied bias magnetic field. Also YIG resonators biased by powerful permanent magnets could have rather high resonance frequencies lying in the GHz frequency range, and demonstrate a relatively low linewidth, and, therefore, a relatively low level of phase noise, especially at the reasonably large offset frequencies from the carrier. Another common method to reduce the oscillator phase noise is to use *voltage-controlled oscillators* (VCOs) stabilized with a phase-locked loop (PLL) [1–3], but, although this technique allows significant reduction of the close-in phase noise, the far-out phase noise still remains determined by the intrinsic parameters of the used VCO.

The phase noise of an oscillator can be estimated using an empirical Leeson equation [4]:

$$\mathcal{L}(\Delta\omega) = 10\log\left\{\frac{FkT}{2P_s}\left[1+\left(\frac{\omega_0}{2Q\Delta\omega}\right)^2\right]\left(1+\frac{\omega_c}{\Delta\omega}\right)\right\}, \tag{1}$$

where ω_0 is the oscillator central (or "carrier") frequency, $\Delta\omega$ is the "offset" frequency, P_s is the signal power, F is the noise factor of the oscillator active element, k is the Boltzmann constant, T is the ambient absolute temperature, Q is the unloaded resonator quality factor, and ω_c is the flicker corner frequency [4]. As it follows from Leeson's equation, Eq. (1), both the "close-in" and the "far-out" levels of the phase noise of an oscillator are,

*Present address: Spintec, France. LitvinenkoAN@gmail.com

 © 2021 American Physical Society

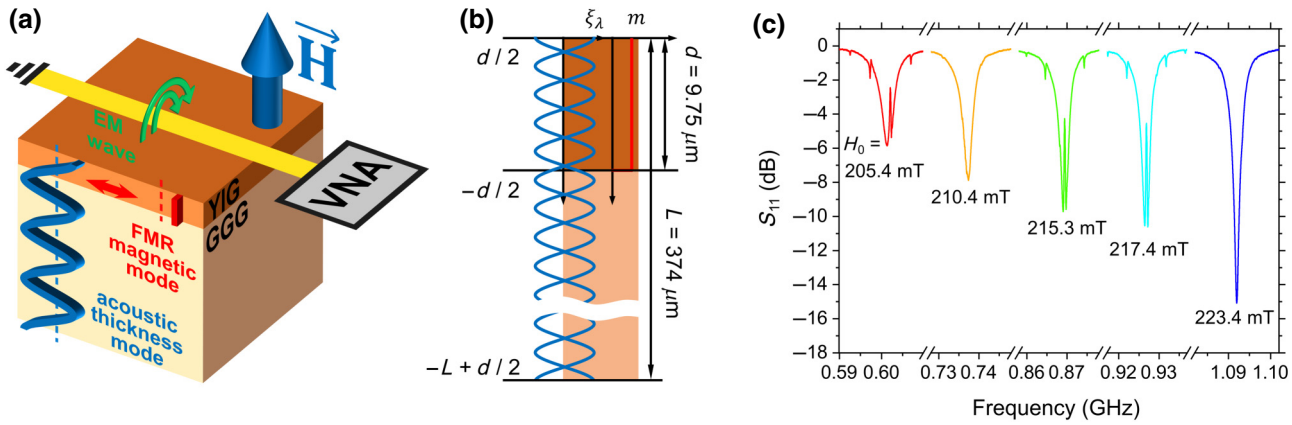

FIG. 1. (a) Scheme of a simple one-port reflection-based MAR, which is experimentally characterized using a vector network analyzer (VNA); (b) thickness distributions of the magnetic FMR mode and standing acoustic modes in the YIG-GGG bilayer sample; (c) S_{11} parameters of the one-port MAR at different values of the perpendicular-to-plane magnetic bias field.

mainly, determined by the quality factor of a resonator used in the oscillator.

Thus, the enhancement of the resonator Q factor is a key element in the development of reference oscillators for information and signal processing [5–8]. This goal, in principle, can be achieved by using resonators with low energy losses, such as dielectric [9], optoelectronic [10], acoustic [11], and magnetic oscillators [12], or the combinations of these oscillator types [13,14].

The highest Q factor, so far, is found in optoelectronic and dielectric resonators, but, unfortunately, these resonator types are, usually, rather bulky and have insufficient thermal stability of their resonance frequency. An alternative is to use the solid-state acoustic resonators that can demonstrate Q factors that are much higher than in magnetic YIG resonators, while having sizes that are much smaller than the sizes of dielectric and optoelectronic resonators and systems. Unfortunately, the purely acoustic resonators are not tunable.

A compromise solution would be to use hybrid magnetoacoustic resonators (MARs) that can support hybrid magnetoelastic oscillation modes that combine a high quality factor of the purely acoustic modes with the excellent tunability of the magnetic modes. It was shown in the 1950s and 1960s that YIG has a considerable magnetostriction constant [15], and that magnetoelastic waves of the GHz frequency range can be efficiently excited in magnetic layered films and heterostructures [16–23]. In the 1980s the technological progress in the liquid-phase epitaxy resulted in the development of high-quality (FMR linewidth below 0.05 mT) YIG films grown on the (almost lattice-matched) monocrystalline gadolinium-gallium-garnet (GGG) substrates. It was also demonstrated that magnetic oscillations excited in YIG through magnetostriction can effectively excite standing acoustic thickness modes in the whole YIG-GGG garnet structure, because the sound velocities in YIG and GGG are almost equal [24–27]. The interest in magnetoacoustic effects in garnet heterostructures has been recently revived in a number of papers where YIG-GGG structures were used either in the transmission-line configuration [28–30] or with ZnO acoustical transducers, which were used for a broadband excitation of acoustic modes in these structures [31–34].

Below, we show that a traditional parallel-plate straight-edge YIG-GGG resonator can be successfully used as a tunable high-Q-factor magnetoacoustic resonance element of a local oscillator with a low phase noise. YIG-GGG films were previously used as hybrid MARs [35,36], where the YIG film served as an effective, narrowband, and frequency-tunable transducer, which can selectively excite an acoustic thickness standing mode of the YIG-GGG structure, having a desirable frequency. In the configuration presented in Fig. 1 the whole YIG-GGG structure acts as an effective high-overtone bulk acoustic resonator (HBAR) [11,37,38]. Note, that HBARs among all the known acoustic resonators demonstrate the highest $Q \times f$ product (up to 10^{14}) [39], making the proposed YIG-GGG MAR design well suited for the realization of low-phase-noise local oscillators. In this work, using the results of theoretical analysis of the magnetoacoustic interaction and experimental parameters of the YIG-GGG epitaxial parallel-plate structures, we design a tunable magnetoacoustic oscillator that has a level of phase noise, that is much lower than in conventional magnetic oscillators based only on the FMR mode of a YIG film.

II. MAGNETOACOUSTIC RESONATOR WITH A HIGH Q FACTOR

The scheme of the YIG-GGG MAR is shown in Fig. 1(a). It consists of a parallel-plate straight-edge rectangular resonator cut from a monocrystalline epitaxial YIG-GGG bilayer magnetized to saturation perpendicular to its plane by a bias magnetic field $\mathbf{H}_0$, and excited by a

strip-line antenna connected to a VNA. The YIG film in the bilayer has the static magnetization $4\pi M_s = 174$ mT, the FMR linewidth $\Delta H_0 = 0.05$ mT, and the thickness of 9.75 μm, and the in-plane sizes of 2×2 mm^2. The thickness of the GGG layer is 364 μm.

A signal of a given frequency f from the strip-line antenna excites the FMR mode in the YIG layer (uniform along the YIG-film thickness) corresponding to a particular magnitude of the bias perpendicular bias magnetic field H_0. The FMR mode of the YIG resonator is coupled through the YIG magnetostriction to the standing thickness acoustic modes of the YIG-GGG heterostructure, and by simultaneous variation of the excitation frequency f and the bias magnetic field H_0 it is possible to align any of the discrete thickness acoustic modes of the YIG-GGG heterostructure with the YIG-resonator FMR frequency given by the Kittel formula:

$$f = \gamma(H_0 - \mu_0 M_s), \tag{2}$$

where $\gamma = 28.3$ GHz/T is a gyromagnetic ratio of YIG.

In Fig. 1(c), the S_{11} parameter of the MAR is shown at different values of bias magnetic field H_0. A distinctive feature of the S_{11} parameter of the MAR is a dip with narrow inverse acoustic peaks. A broadband dip belongs to the FMR mode of the YIG film, while the narrow acoustic peaks, which appear at bias field H_0 values of 205.4, 215.3, and 217.4 mT, correspond to the high-overtone magnetoacoustic resonances in the YIG-GGG structure. Note, also that there are frequencies and corresponding bias field values at which acoustic peaks do not appear within the FMR dip. This indicates the absence of the magnetoacoustic coupling.

To analyze the magnetoacoustic coupling in the proposed structure as a function of the frequency and the acoustic mode number we employ the theoretical description of the magnetoacoustic interaction in the sample (Fig. 1) developed in Refs. [40,41]. We start with the density of magnetoelastic energy in the form:

$$W = W_{\text{mag}} + W_{\text{el}} + W_{\text{mel}}. \tag{3}$$

Here W_{mag} is the density of magnetic energy, which includes contributions from the Zeeman, exchange and magnetodipolar interactions; $W_{\text{el}} = \left[\rho\,(d\xi/dt)^2 + c_{iklm}u_{ik}u_{lm}\right]/2$ is the elastic energy with the tensor of elastic constants c_{iklm} and $u_{ik} = (d\xi_i/dx_k + d\xi_k/dx_i)/2$, ξ is an acoustic displacement, and ρ is the density of the material; $W_{\text{mel}} = b_{iklm}M_iM_ku_{lm}/M_s^2$ is the magnetoelastic interaction with the tensor of magnetostriction constants b_{iklm} [42].

Using the expression for the energy in Eq. (3), one can write two coupled equations for the elastic displacement ξ and magnetization $\mathbf{M}$ as

$$\rho\frac{\partial^2\xi_m}{\partial t^2} = \frac{\partial}{\partial x_l}\frac{\partial W}{\partial u_{lm}} = \frac{b_{iklm}}{M_s^2}\frac{\partial M_i}{\partial x_l}M_k + c_{iklm}\frac{\partial u_{ik}}{\partial x_l}, \tag{4}$$

$$\frac{d\mathbf{M}}{dt} = -\gamma\left[\mathbf{M}\times\left(\mathbf{H}^{\text{mag}} + \mathbf{H}^{\text{mel}}\right)\right], \tag{5}$$

where $\mathbf{H}^{\text{mag}} = \partial W_{\text{mag}}/\partial\mathbf{M}$ and $H_i^{\text{mel}} = 2b_{iklm}M_ku_{lm}/M_s^2$.

Below we represent the magnetization vector $\mathbf{M}$ as a sum of its static and precessional (dynamic) parts, and the latter is expressed as the FMR mode of the thin YIG film:

$$\mathbf{M} = M_s\left[\boldsymbol{\mu}_0 + \mathbf{m}a(t)e^{-(i\omega_0+\Gamma)t} + \text{c.c.}\right], \tag{6}$$

where ω_0 and Γ are the angular frequency and damping parameter of the FMR mode.

In our case the static magnetization of YIG $\boldsymbol{\mu}_0$ is perpendicular to the film plane, while the dynamic magnetization $\mathbf{m} \perp \boldsymbol{\mu}_0$ describes the spatial (thickness) profile of the FMR mode in the absence of the magnetoelastic interaction $\mathbf{H}^{ac} = 0$. Similarly, we represent the dynamic acoustic displacement, using the known profiles of the acoustic thickness eigenmodes of the YIG-GGG structure:

$$\boldsymbol{\xi}(z) = \sum_\lambda \tilde{\boldsymbol{\xi}}_\lambda(z)b_\lambda(t)e^{-(\tilde{\Gamma}+i\tilde{\omega}_\lambda)t} + \text{c.c.} \tag{7}$$

Taking into account the following orthogonality relations for magnetic and acoustic modes:

$$\frac{M_s}{\gamma}\int_{-d/2}^{d/2}\mathbf{m}^*(\boldsymbol{\mu}_0\times\mathbf{m})dz = -iA, \tag{8}$$

$$2\rho\omega_\lambda\int_{-L+d/2}^{d/2}\tilde{\boldsymbol{\xi}}_\lambda^*\tilde{\boldsymbol{\xi}}_{\lambda'}dz = Q_\lambda\delta_{\lambda\lambda'}, \tag{9}$$

where $A > 0$ and $Q_\lambda > 0$ are the spin-wave and acoustic normalization constants having the dimensionality of action [40]. One can rewrite Eqs. (4) and (5) as

$$\begin{aligned} &A\left[\dot{a}(t) + i\omega a(t) + \Gamma_0 a(t)\right] = i\kappa_\lambda b(t),\\ &B_\lambda\left[\dot{b}_\lambda(t) + i\tilde{\omega}_\lambda b_\lambda(t) + \tilde{\Gamma}_\lambda b_\lambda(t)\right] = i\kappa_\lambda^* a(t), \end{aligned} \tag{10}$$

where we introduce in a common way [40,43,44] the damping rates of the spin and acoustic modes Γ_0 and $\tilde{\Gamma}_\lambda$, respectively, as well as the coupling constant defined by the expression:

$$\kappa_\lambda^2 = \frac{b^2\gamma}{2\omega_\lambda\rho M_sLd}\left|\int\mu_0\mathbf{m}^*\frac{\partial\tilde{\boldsymbol{\xi}}_\lambda}{\partial z}dz\right|^2, \tag{11}$$

where $b = b_{1111} - b_{1122}$. If $\mathbf{m}$ and $\boldsymbol{\xi}$ describe plane waves (i.e., magnons and phonons), the coefficient κ defines the bandgap at the point of avoided crossing (hybridization) of their spectra. In our case κ^2 defines the part of the oscillator "energy" involved in the magnetoelastic interaction. Note that the interaction coefficient κ is expressed in the

units of frequency, i.e., it is defined in relation to the central (carrier) frequency of the MAR.

We assume that the thickness profiles of both the FMR magnetic mode $\tilde{m}$ and the standing acoustic modes $\tilde{\xi}_\lambda$ satisfy the "free" (or "unpinned") boundary conditions at the both parallel-plate surfaces and at the YIG-GGG interface:

$$\tilde{m} = 1, \qquad \tilde{\xi}_\lambda(z) = \cos\left[(z - d/2)\,\pi\lambda/L\right], \tag{12}$$

For the spatially uniform static magnetization in the YIG layer with a sufficiently sharp transition at the YIG-GGG interface one can write $\mu_0(z) = \Theta(d/2 + z)\Theta(d/2 - z)$ and $m(z) = \tilde{m}\Theta(d/2 + z)\Theta(d/2 - z)$, where $\Theta(z)$ means Heaviside θ function.

Finally, for the coupling coefficient [45] we obtain

$$\kappa_\lambda^2 = \frac{\gamma b^2}{2\pi^2 d\lambda M_s\sqrt{c_{44}\rho}}\left(1 - \cos\frac{\pi\lambda d}{L}\right)^2, \tag{13}$$

where c_{44} is the elastic modulus of YIG [46].

The theoretically calculated coupling coefficient for the YIG-GGG sample used in our experiments is shown in Fig. 2(a) (black open circles). As can be seen from the figure, the coupling coefficient κ demonstrates an oscillating behavior: the overlap integral between the thickness profiles of the FMR mode and the acoustic modes has local maxima when there are $n/2$ acoustic wavelength over the thickness of the YIG film, and this integral vanishes to zero when there are $(n+1)/2$ acoustic wavelengths over the thickness of the YIG layer. The oscillations in the magnitude of the coupling coefficient reduce the operating range of frequencies for the MAR. As follows from the theory, in order to increase the period of oscillations of the coupling coefficient κ and extend the operating frequency range of the MAR, one has to reduce the thickness of the YIG film.

The magnetoelastic coupling can be described using a Darko Kajfez's method [47] modified for hybrid MAR having two resonant subsystems (see description in Appendix B). The experimentally measured oscillations in the magnetoelastic coupling have the same period as the ones calculated theoretically. This agreement between the theory and the experiment confirms that in the proposed structure of a MAR, the FMR mode, indeed, excites the acoustic modes of the YIG-GGG structure.

These acoustic modes we attribute to shear acoustic waves propagating deep into the GGG substrate. It

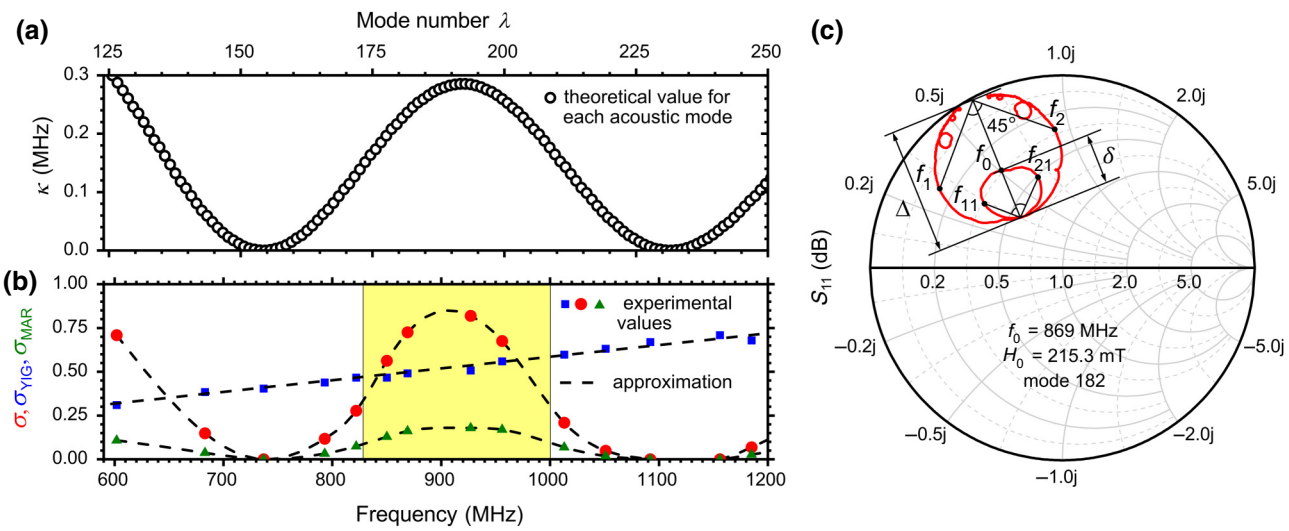

FIG. 2. Coupling coefficients in the MAR as functions of the excitation frequency and the excited acoustic mode number λ: (a) theoretically calculated coupling coefficient between the FMR mode of the YIG resonator and the thickness acoustic modes of the YIG-GGG structure; (b) experimentally measured coupling coefficients: $\sigma_{\rm YIG}$ between the strip-line line and the FMR mode of the YIG resonator (blue squares); σ between the FMR mode of the YIG resonator and the acoustic thickness modes of the YIG-GGG structure (red circles), $\sigma_{\rm MAR}$ overall coupling between the strip-line and the acoustic thickness modes (green triangles). The region highlighted in yellow indicates the frequency band where the overall coupling coefficient is suitable for the operation of the oscillator scheme. Note, that the FMR frequency of the YIG resonator is adjusted for a particular acoustic mode by changing the bias magnetic field H_0. In the frame (c), the experimental S_{11} parameter at the magnetic field $H_0 = 215.3$ mT and in the frequency band 869 ± 15 MHz is plotted on the Smith charts. The main loop with a diameter Δ corresponds to the FMR mode, while inner loops correspond to acoustic modes. The central inner loop with a diameter δ corresponds to the acoustic mode with which the FMR frequency is aligned. The values of Δ, δ are used to calculate the experimental values of $\sigma_{\rm YIG}$, $\sigma_{\rm MAR}$, σ, while the frequencies $f_0, f_1, f_2, f_{11}, f_{22}$ are used to calculate the Q factors $Q_{\rm YIG}, Q_{\rm MAR}$, as described in Appendix B. At the frequencies where the coupling coefficient δ is close to zero, the inner acoustic loops disappear from the MAR S_{11} parameter diagram.

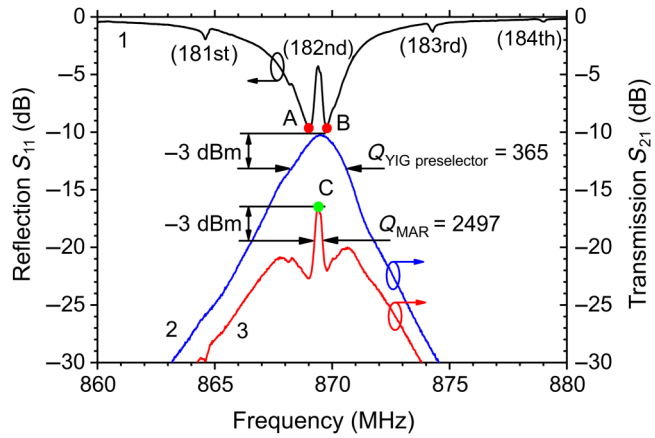

FIG. 3. S parameters of the one-port (see Fig. 1) and two-port composite (Fig. 4) MARs: black line, S_{11} parameter of the one-port MAR and S_{21}parameter of a two-port MAR; blue line, S_{21} parameter of the FMR-based preselector; red line, S_{21} parameter of the composite two-port MAR. The mode numbers of a corresponding acoustic thickness modes in the YIG-GGG parallel plate are given in brackets. Points A, B, and C are where the Barkhausen criterion for stable auto-oscillations is satisfied.

was experimentally shown in Ref. [24], that in such a YIG-GGG structure the peaks of longitudinal wave modes have much lower intensity as compared to shear wave modes. In our case the excitation intensity of longitudinal wave modes is also negligibly small so that those peaks are practically unnoticeable in Fig. 3.

Due to the relatively high value of YIG resonator Q factor $Q_{\text{YIG}} \approx 200 - 400$ the frequency bandwidth of the FMR in a laterally constrained YIG resonator is narrower, than the frequency spacing between the acoustic thickness modes of the YIG-GGG structure $\Delta f_a = V_a/(2L) =$ 4.773 MHz, where $V_a = 3.57 \times 10^5$ cm/s is the velocity of transverse acoustic waves in GGG (for comparison, the transverse acoustic wave velocity in YIG is $V_a = 3.84 \times 10^5$ cm/s). With this the YIG-film resonator can selectively excite a single acoustic shear mode of the YIG-GGG structure without using any narrowband external filters. A YIG-GGG MAR can be tuned to excite effectively a single acoustic resonance mode having numbers from 173 to 208 in the [840 MHz : 1.0 GHz] frequency band with the step $\Delta f_a = 4.773$ MHz by changing the magnitude of the bias magnetic field H_0 applied to the YIG film.

Since the YIG film works as a transducer between the electric signals in the strip-line antenna and the acoustic thickness modes, the overall coupling coefficient between strip-line and acoustic modes has to be taken into account for the oscillator design. The overall coupling coefficient is shown in the Fig. 2(b). The detailed description on how to obtain experimental coupling coefficients of the hybrid YIG-GGG resonator is given in Appendix B.

III. DESIGN OF A MAGNETOACOUSTIC OSCILLATOR

A useful parameter for the design of an oscillator, which employs high-overtone resonators is the mode selectivity. In order to get stable oscillations without modulations and random spurs in the phase-noise characteristic one has to make sure that when a particular mode is selected to be resonant, the damping of the adjacent modes is sufficiently strong. For the above described MAR, the selectivity depends on the frequency separation between acoustic modes and on the linewidth of the FMR mode of the YIG layer.

Using our experimental data, we find that when the frequency of the FMR mode of the MAR is tuned for the resonant acoustic mode having number 182, its coupling coefficient with this mode is 3.5 times larger than the corresponding coupling coefficients with the adjacent acoustic modes having numbers 181/183. The caulking advantage for the chosen resonant acoustic mode can be further increased if an additional YIG preselector is used. Moreover, with the increase of the central frequency of the MAR the loaded Q factor of the magnetic (YIG) resonator grows linearly and, therefore, the effective linewidth of the YIG-FMR mode decreases, thus increasing selectivity of the MAR.

The basic principles of the design of an efficient magnetoacoustic oscillator can be understood from the analysis of the experimental S-parameter data presented in Fig. 3. First of all, let us look at the experimentally measured overall coupling coefficient of the one-port simple MAR presented in Fig. 1 (green triangles in Fig. 2). In the experience of practical oscillator design, the minimal coupling coefficient between the oscillator core and the resonator should be above 0.1 for high stability and low phase noise. Therefore, according to this empirical condition the oscillator based on the MAR can operate in the range of frequencies between 0.84 and 1 GHz (see the region highlighted in yellow in Fig. 2). For further design steps we choose the resonance acoustic mode within a yellow region having number 182, and the Q factor of $Q_{\text{MAR}} = 2497$. As discussed earlier, the resonance characteristic of a one-port reflection-based MAR has an unusual form of a dip, caused by the FMR in the YIG layer with an inverted central peak in the middle attributed to the resonance acoustic mode with the number 182 of the whole YIG-GGG structure. The analysis, however, shows that if we use a conventional one-port reflection-based oscillator design, the Barkhausen stability criterion for the auto-oscillations is only satisfied at points A and B (which are situated outside of the central peak of the acoustic resonance for mode 182, see Fig. 3). Therefore, the use of such a design for a magnetoacoustical oscillator (MAO) will not substantially decrease the MAO phase-noise figure, since the phase noise will, mostly, be determined by a relatively low Q factor of the FMR mode.

Moreover, in the systems where several competing resonance modes (corresponding to points A and B on the black curve) can be excited simultaneously it is possible to have mode bistability and chaotic dynamics [48].

In order to take full advantage of the high Q factor of a *single acoustic resonance mode*, a special scheme based on the one-port MAR is designed to satisfy the Barkhausen stability criterion near the frequency of the acoustic resonance mode. It is done in two steps. First, a circulator is added serially to the one-port MAR forming a two-port circuit, which has a S_{21} parameter absolutely identical to a S_{11} parameter of the one-port MAR. For a ring oscillator scheme based on such a two-port circuit (see a part of the scheme between point 1 and 3) given an adjusted open-loop phase and amplification the Barkhausen stability criterion would be satisfied at the same time at the narrow peak corresponding to the frequency of the acoustic resonance and at frequencies far from the FMR dip. Therefore, in a second step we introduce an additional purely magnetic two-port YIG resonator patterned on the same GGG substrate as a preselector bandpass filter (having a *scratched bottom GGG surface* to prevent the formation of the standing acoustic thickness modes), which suppresses the signal at frequencies outside of the FMR resonance. As a result of such a design, the transmission (S_{21}) characteristic of the composite two-port MAR (red line in Fig. 3) is approximately a product of the transmission characteristic of the two-port circuit based on the MAR and a circulator (black curve in Fig. 3), and the transmission characteristic of the FMR-based preselector (blue curve in Fig. 3). As a result the transmission characteristic of the composite two-port MAR (Fig. 4) has a usual form of a resonance characteristic with a central maximum. We note, that a MAR transmission characteristic with a central maximum, similar to the one shown by the red curve in Fig. 3, can be obtained by simpler means in a three-layer YIG-GGG-YIG structure, which was used in Ref. [36], without use of an additional preselector. However, in that case the thickness of the GGG layer can not be adjusted by polishing, and the frequency spacing of the acoustic thickness modes can not be adjusted after the growth of the YIG layers by liquid epitaxy. Another limitation is that the liquid-epitaxy process requires the GGG-substrate thickness to be at least 300 μm, while with polishing of one-sided YIG-GGG structure this thickness can be reduced down to 50-100 μm, thus increasing the operational frequency range of the MAR.

Finally, to complete the scheme of MAO a low-phase-noise amplifier ABA-54563 is added (see the circuit Fig. 4) to compensate losses in the oscillator feedback loop. A phaseshifter in the form of a variable delay line is used to obtain the correct phase shift ($2\pi n$, where $n = 0, 1, 2 \ldots$) in the loop to satisfy the phase condition of the Barkhausen stability criterion for the auto-oscillations. A variable attenuator is introduced to limit the signal power at the input of the MAR to suppress the nonlinearities and avoid the increase of the phase noise. Finally, a coupler is used to extract the output signal. Given the adjusted amplification, phase shift in the feedback loop, and the bias magnetic field applied to the YIG film, the auto-oscillation conditions for the composite two-port MAR are satisfied only at the frequency of the acoustic thickness mode having the number 182 and the effective Q factor of 2497 (see point C in Fig. 3). Moreover, the adjacent acoustic thickness mode with the number 181 is suppressed by 13 dB as compared to the resonant mode with the number 182. Thus, a single-mode auto-oscillation regime based on the high-Q-factor acoustic thickness mode in a composite two-port MAR is realized.

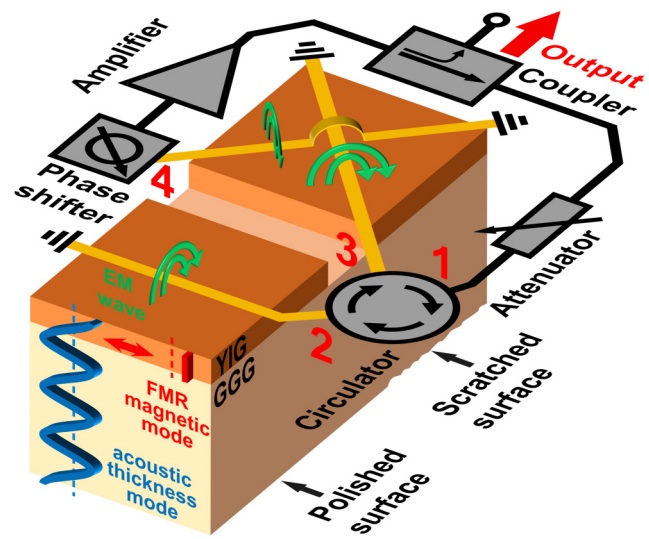

FIG. 4. Scheme of a MAO based on a composite two-port MAR consisting of a one-port YIG-GGG MAR (left part of a YIG layer) connected to a YIG-FMR-based preselector filter (right part of the YIG layer). The left part in connection with a circulator forms a two-port MAR, which is connected to the purely magnetic YIG-FMR-based preselector filter formed by the right part of the YIG layer, where the acoustic modes are eliminated by scratching the bottom surface of the GGG substrate.

IV. RESULTS ON LOW PHASE NOISE

The experimentally measured phase-noise figure of an auto-oscillator based on the composite two-port MAR (see Fig. 4) having ($Q_{\mathrm{MAR}} = 2497$) is presented in Fig. 5 by a red curve. In the same figure, for comparison, we show by the blue curve the experimentally measured phase-noise figure for an auto-oscillator based on a purely magnetic YIG-FMR preselector oscillator ($Q_{\mathrm{YIG}} = 365$). The theoretical estimations of the phase-noise figures in these two auto-oscillators obtained from Eq. (1) are shown in Fig. 5 by the black dashed line and the black dotted line, respectively.

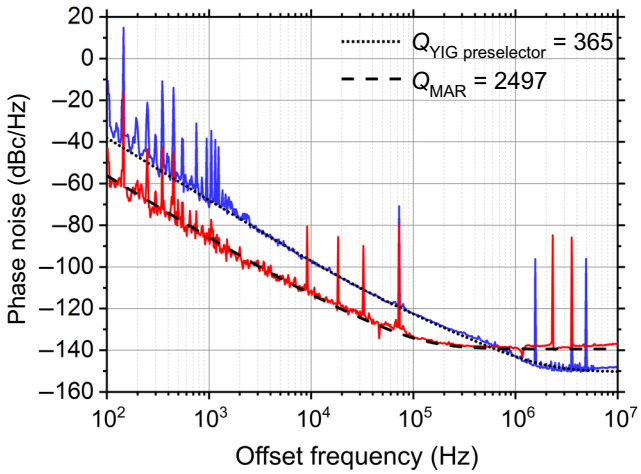

FIG. 5. Experimentally measured phase-noise figures for auto-oscillators based on a purely magnetic YIG-FMR resonator (blue line) and on a composite two-port magnetoacoustic YIG-GGG resonator (red line). Dotted black line shows the estimation of the phase noise obtained from Leeson's formula, Eq. (1), for a FMR-based magnetic preselector resonator ($Q_{\mathrm{YIG}} = 365$), while the dashed black line shows a similar estimation of a phase noise for the composite two-port MAR (Fig. 4) having the Q factor $Q_{\mathrm{MAR}} = 2497$.

The phase noise of the MAO based on the composite two-port MAR is −87 dBc/Hz at the 1-kHz offset and −116 dBc/Hz at the 10-kHz offset, which is at least 20 dB better than the phase-noise figure of a conventional auto-oscillator based on a YIG-FMR resonator. Note, at the same time, that at large off-set frequencies the phase noise of an auto-oscillator based on a composite two-port MAR degrades, and becomes higher than in the case of a conventional YIG-FMR oscillator. This increase in the MAO phase noise is caused, mainly, by the presence of a variable attenuator in the MAO scheme (Fig. 4), which is introduced to avoid saturation of the one-port MAR in nonlinear mode. Note, also, that the nonlinearity threshold of the one-port MAR is lower, than of the YIG-FMR two-port resonator. We want to mention that instead of combination of the amplifier ABA-54563 with the variable attenuator, an amplifier with a lower saturation power level can be used in the MAO design scheme to reduce the maximum power level of a self-sustained signal at the one-port MAR input while still having high small-signal amplification in the loop, which altogether reduces the noise factor of the feedback loop. This will improve the phase-noise figure in the whole range of offset frequencies.

V. CONCLUSION

We show that the FMR mode excited in a YIG layer of a parallel-plate YIG-GGG heterostructure can be effectively coupled to the high-Q-factor standing-thickness acoustic modes of the YIG-GGG bilayer. The frequency dependence of this magnetoelastic coupling is studied both theoretically and experimentally, and the optimum conditions for this coupling corresponding to the stable single-mode auto-oscillations are found. A composite two-port MAR based on the YIG-GGG heterostructure is developed and practically realized, and the phase-noise figure in the auto-oscillator based on the developed MAR is substantially improved, in comparison with the auto-oscillator based on the conventional YIG-FMR two-port resonator. We want to stress, that the advantage of using shear acoustic modes in the developed MAR over the longitudinal acoustic waves in conventional HBARs is caused by the fact that shear acoustic waves are insensitive to the amorphous load as they propagate only in solids. This property provides a significant simplification of technological requirements for the manufacturing of the proposed composite MARs.

In summary, we design a composite magnetoacoustic auto-oscillator with a low phase noise based on a parallel-plate YIG-GGG bilayer. The relatively narrow FMR linewidth of the YIG layer provides the possibility for selective resonance excitation of a single acoustic thickness mode of the YIG-GGG structure and, therefore, makes possible a significant improvement of the Q factor of the resulting MAR. The phase-noise figure of the auto-oscillator based on the developed composite MAR is −87 dBc/Hz at 1-kHz offset and −116 dBc/Hz at 10-kHz offset, which is at least 20 dB better than the performance of the auto-oscillating scheme based on a conventional YIG-FMR two-port resonator. The designed MAO can be used in the frequency-agile data transmission where abrupt frequency hopping is employed. As an outlook, we note that the microwave circulator used in our scheme of the composite two-port MAR can be replaced with a matching circuit or an active component to make the developed MAR CMOS compatible.

ACKNOWLEDGMENTS

This work is supported by the Grant of the Government of the Russian Federation for supporting scientific research projects supervised by leading scientists at Russian institutions of higher education (Contract No. 11.G34.31.0030) and supported in part by the U.S. National Science Foundation (Grant No. EFMA-1641989), by the U.S. Air Force Office of Scientific Research under the MURI Grant No. FA9550-19-1-0307, and by the Oakland University Foundation. The work of S.A.N. is supported by Agreement with Ministry of Science and Higher Education of the Russian Federation Grant No. 13.1902. 21.0010.

We thank Dr. Olivier Klein for help with the precise measurement of the YIG and GGG thickness using interferometry technique.

APPENDIX A: DEVICE FABRICATION

The design of the one-port reflection-type MAR and the composite two-port MAR are shown in Fig. 1 and Fig. 4, correspondingly. Both resonators are manufactured using a two-layer parallel-plate YIG-GGG structure with the YIG thickness of $d = 9.75$ μm, GGG thickness of $L = 364$ μm, and YIG saturation magnetization of $M_0 = 1740/(4\pi)$Oe. The chemical-mechanical polishing technique is used to create the highly parallel surfaces of YIG-GGG structure with the wedge angle less than $2''$, which ensures the formation of high-overtone acoustic thickness resonances in the YIG-GGG structure. The fabricated sample of the one-port MAR had the lateral dimensions of 1×1 mm. The composite two-port MAR is fabricated by the means of laser-scribing technique [49] and has lateral dimensions of 1×2.5 mm. The inner surface of the two-port YIG preselector film of the composite two-port MAR is scratched with a micromesh wet-sanding abrasive paper having grit 3200 to eliminate acoustic resonances as they would counteract those in the one-port MAR.

APPENDIX B: DEVICE CHARACTERIZATION

The developed MAR and the YIG preselector FMR resonator are characterized using Keysight (Agilent E8361A) vector network analyzer. The phase noise of the developed composite MAO is measured using a signal-source analyzer (Keysight E5052B).

The experimental method used for the characterization of the magnetoacoustic coupling in the MAR is a modified Darko Kajfez's method. This method is based on the analysis of the resonance loops in a S_{11}-parameter graph plotted on a Smith chart. This method gives dimensionless values of the loaded Q factors, and coupling coefficients that define interaction of electrical subsystems in the filter theory. To obtain the S_{11} parameter of the MAR we use the electrical setup shown in Fig. 1(a). The strip-line antenna used in our experiments has a width of 0.5 mm, which is comparable to the sample size, and ensures an efficient excitation of the FMR mode. In order to obtain the loaded Q factors and coupling coefficients of the one-port MAR some additional geometrical constructions are used on the Smith chart. First, to get the parameters of a magnetic resonator, three lines have to be drawn from the node of the big loop, as shown in Fig. 2(c): one line goes through the center of the loop, while two other lines go at the angle of 45° to each side of the center line. This allows us to extract from the S-parameter measurement the values of the corresponding frequencies f_1, f_2, and f_0 as the intersection points between the auxiliary lines and the S-parameter curve. The interval $f_2 - f_1$ defines the FMR linewidth, and is used to calculate the loaded Q factor of the YIG magnetic resonator:

$$Q_{\mathrm{YIG}} = \frac{f_0}{f_2 - f_1}. \tag{B1}$$

Similar geometric constructions are made with the largest inner loop, in order to obtain the frequencies f_{11}, f_{21}, which define the width of the resonant acoustic mode of the YIG-GGG structure, and its loaded Q factor:

$$Q_{\mathrm{MAR}} = \frac{f_0}{f_{21} - f_{11}}. \tag{B2}$$

In order to calculate the coupling coefficients between the subsystems in the MAR one should measure the diameter of the main resonance loop and the largest inner loop. The coupling between the strip-line and the YIG-FMR magnetic resonator is defined by the expression:

$$\sigma_{\mathrm{YIG}} = \frac{\Delta}{2R - \Delta}, \tag{B3}$$

where $2R = 2$ is a radius of the Smith chart. The overall coupling between the strip-line and the acoustic subsystem can be obtained using a similar formula:

$$\sigma_{\mathrm{MAR}} = \frac{\delta}{2R - \delta}. \tag{B4}$$

In order to compare the theoretically calculated κ with the experimental data we introduce a coupling coefficient σ, which provides a measure of coupling between the magnetic and acoustic subsystems:

$$\sigma = \frac{\delta}{\Delta - \delta}. \tag{B5}$$

Detailed explanation and derivation of the expressions presented above can be found in Ref. [47].

[1] R. L. Carter, J. M. Owens, and D. K. De, YIG oscillators: Is a planar geometry better? (short papers), IEEE Trans. Microw. Theory Tech. **32**, 1671 (1984).

[2] A. Chenakin, Select a VCO or YIG for a PLL synthesizer? Microw. RF **50**, 72 (2011).

[3] R. E. Best, *Phase-Locked Loops* (McGraw Hill, New York, 2007).

[4] D. B. Leeson, A simple model of feedback oscillator noise spectrum, Proc. IEEE **54**, 329 (1966).

[5] A. Vorobiev and S. Gevorgian, Tunable thin film bulk acoustic wave resonators with improved Q-factor, Appl. Phys. Lett. **96**, 212904 (2010).

[6] K. Geerlings, S. Shankar, E. Edwards, L. Frunzio, R. J. Schoelkopf, and M. H. Devoret, Improving the quality factor of microwave compact resonators by optimizing their

geometrical parameters, Appl. Phys. Lett. **100**, 192601 (2012).

[7] W. Xu, X. Zhang, H. Yu, A. Abbaspour-Tamijani, and J. Chae, In-liquid quality factor improvement for film bulk acoustic resonators by integration of microfluidic channels, IEEE Electron Dev. Lett. **30**, 647 (2009).

[8] D.-P. Cai, J.-H. Lu, C.-C. Chen, C.-C. Lee, C.-E. Lin, and T.-J. Yen, High Q-factor microring resonator wrapped by the curved waveguide, Sci. Rep. **5**, 10078 (2015).

[9] D. Kajfez and P. Guillon, *Dielectric Resonators* (Artech House Inc., Norwood, MA, 1986), p. 547. No individual items are abstracted in this volume (1986).

[10] K. Volyanskiy, J. Cussey, H. Tavernier, P. Salzenstein, G. Sauvage, L. Larger, and E. Rubiola, Applications of the optical fiber to the generation and measurement of low-phase-noise microwave signals, JOSA B **25**, 2140 (2008).

[11] K. M. Lakin, G. R. Kline, and K. T. McCarron, High-Q microwave acoustic resonators and filters, IEEE Trans. Microw. Theory Tech. **41**, 2139 (1993).

[12] E. Bankowski, T. Meitzler, R. S. Khymyn, V. S. Tiberkevich, A. N. Slavin, and H. X. Tang, Magnonic crystal as a delay line for low-noise auto-oscillators, Appl. Phys. Lett. **107**, 122409 (2015).

[13] V. Vitko, A. Nikitin, A. Ustinov, and B. Kalinikos, A theoretical model of dual tunable optoelectronic oscillator, J. Phys.: Conf. Ser. **1038**, 012106 (2018).

[14] M. M. Torunbalci, T. A. Gosavi, K. Y. Camsari, and S. A. Bhave, Magneto acoustic spin hall oscillators, Sci. Rep. **8**, 1 (2018).

[15] R. Comstock, Magnetoelastic coupling constants of the ferrites and garnets, Proc. IEEE **53**, 1508 (1965).

[16] C. Kittel, Interaction of spin waves and ultrasonic waves in ferromagnetic crystals, Phys. Rev. **110**, 836 (1958).

[17] E. G. Spencer and R. LeCraw, Magnetoacoustic Resonance in Yttrium Iron Garnet, Phys. Rev. Lett. **1**, 241 (1958).

[18] J. R. Eshbach, Spin-wave propagation and the magnetoelastic interaction in yttrium iron garnet, J. Appl. Phys. **34**, 1298 (1963).

[19] E. Schlömann and R. I. Joseph, Generation of spin waves in nonuniform magnetic fields. III. Magnetoelastic interaction, J. Appl. Phys. **35**, 2382 (1964).

[20] W. Strauss, Magnetoelastic waves in yttrium iron garnet, J. Appl. Phys. **36**, 118 (1965).

[21] B. Auld, J. Collins, and D. Webb, Excitation of magnetoelastic waves in YIG delay lines, J. Appl. Phys. **39**, 1598 (1968).

[22] S. M. Rezende and F. R. Morgenthaler, Magnetoelastic waves in time-varying magnetic fields. I. Theory, J. Appl. Phys. **40**, 524 (1969).

[23] H. Matthews and H. van de Vaart, Magnetoelastic love waves, Appl. Phys. Lett. **15**, 373 (1969).

[24] Y. V. Gulyaev, P. E. ZilBerman, G. T. Kazakov, V. G. Sysoev, V. V. Tikhonov, Y. A. Filimonov, B. P. Nam, and A. S. Khe, Observation of fast magnetoelastic waves in thin yttrium-iron garnet wafers and epitaxial films, Soviet J. Exp. Theor. Phys. Lett. **34**, 477 (1981).

[25] G. Kazakov, V. Tikhonov, and P. Zilberman, Magnetodipole and elastic wave resonance interaction in YIG plates and films, Fiz. Tverd. Tela **25**, 2307 (1983).

[26] P. Zilberman, G. Kazakov, and V. Tikhonov, Self-modulation of fast magnetoelastic waves in yttrium iron garnet films, Tech. Phys. Lett. **11**, 769 (1985).

[27] Y. V. Gulyaev and P. ZilBerman, Magnetoelastic waves in ferromagnet plates and films, Soviet Phys. J. **31**, 860 (1988).

[28] M. Weiler, H. Huebl, F. S. Goerg, F. D. Czeschka, R. Gross, and S. T. B. Goennenwein, Spin Pumping with Coherent Elastic Waves, Phys. Rev. Lett. **108**, 176601 (2012).

[29] P. Chowdhury, P. Dhagat, and A. Jander, Parametric amplification of spin waves using acoustic waves, IEEE Trans. Magn. **51**, 1 (2015).

[30] Y. V. Khivintsev, V. K. Sakharov, S. L. Vysotskii, Yu A. Filimonov, A. I. Stognii, and S. A. Nikitov, Magnetoelastic waves in submicron yttrium–iron garnet films manufactured by means of ion-beam sputtering onto gadolinium–gallium garnet substrates, Tech. Phys. **63**, 1029 (2018).

[31] N. Polzikova, S. Alekseev, I. Kotelyanskii, A. Raevskiy, and Y. Fetisov, Magnetic field tunable acoustic resonator with ferromagnetic-ferroelectric layered structure, J. Appl. Phys. **113**, 17C704 (2013).

[32] I. Pyataikin, N. Polzikova, S. Alekseev, I. Kotelyanskii, V. Luzanov, A. Raevskiy, and L. Galchenkov, Spin pumping in a composite high overtone bulk acoustic wave resonator, Bulletin of the Russian Academy of Sciences: PhysicsBull. Russ. Acad. Sci.: Phys. **81**, 962 (2017).

[33] N. Polzikova, S. Alekseev, V. Luzanov, and A. Raevskiy, Acoustic excitation and electrical detection of spin waves and spin currents in hypersonic bulk waves resonator with YIG/Pt system, J. Magn. Magn. Mater. **479**, 38 (2019).

[34] S. G. Alekseev, S. E. Dizhur, N. I. Polzikova, V. A. Luzanov, A. O. Raevskiy, A. P. Orlov, V. A. Kotov, and S. A. Nikitov, Magnons parametric pumping in bulk acoustic waves resonator, Appl. Phys. Lett. **117**, 072408 (2020).

[35] A. N. Litvinenko, A. V. Sadovnikov, V. V. Tikhonov, and S. A. Nikitov, Brillouin light scattering spectroscopy of magneto-acoustic resonances in a thin-film garnet resonator, IEEE Magn. Lett. **6**, 1 (2015).

[36] K. An, A. N. Litvinenko, R. Kohno, A. A. Fuad, V. V. Naletov, L. Vila, U. Ebels, G. de Loubens, H. Hurdequint, N. Beaulieu, J. Ben Youssef, N. Vukadinovic, G. E. W. Bauer, A. N. Slavin, V. S. Tiberkevich, and O. Klein, Coherent long-range transfer of angular momentum between magnon kittel modes by phonons, Phys. Rev. B **101**, 060407(R) (2020).

[37] R. Boudot, G. Martin, J.-M. Friedt, and E. Rubiola, Frequency flicker of 2.3 GHz ALN-sapphire high-overtone bulk acoustic resonators, J. Appl. Phys. **120**, 224903 (2016).

[38] H. Yu, C. Lee, W. Pang, H. Zhang, A. Brannon, J. Kitching, and E. S. Kim, Hbar-based 3.6 GHz oscillator with low power consumption and low phase noise, IEEE Trans. Ultrason. Ferroelectr. Freq. Control **56**, 400 (2009).

[39] K. M. Lakin, Thin film resonator technology, IEEE Trans. Ultrason. Ferroelectr. Freq. Control **52**, 707 (2005).

[40] R. Verba, I. Lisenkov, I. Krivorotov, V. Tiberkevich, and A. Slavin, Nonreciprocal Surface Acoustic Waves in Multilayers with Magnetoelastic and Interfacial Dzyaloshinskii-Moriya Interactions, Phys. Rev. Appl. **9**, 064014 (2018).

[41] I. Lisenkov, A. Jander, and P. Dhagat, Magnetoelastic parametric instabilities of localized spin waves induced by traveling elastic waves, Phys. Rev. B **99**, 184433 (2019).

[42] S. Chikazumi, *Physics of Ferromagnetism*, International Series of Monographs on Physics (OUP Oxford, New York, 2009).

[43] R. Verba, G. Melkov, V. Tiberkevich, and A. Slavin, Collective spin-wave excitations in a two-dimensional array of coupled magnetic nanodots, Phys. Rev. B **85**, 014427 (2012).

[44] R. Fleury, D. L. Sounas, C. F. Sieck, M. R. Haberman, and A. Alù, Sound isolation and giant linear nonreciprocity in a compact acoustic circulator, Science **343**, 516 (2014).

[45] A. Brataas, B. van Wees, O. Klein, G. de Loubens, and M. Viret, Spin insulatronics, Phys. Rep. **885**, 1 (2020).

[46] A. Borovik-Romanov and S. Sinha, *Spin Waves and Magnetic Excitations*, ISSN (Elsevier Science, Amsterdam, 2012).

[47] D. Kajfez and E. J. Hwan, Q-factor measurement with network analyzer, IEEE Trans. Microw. Theory Tech. **32**, 666 (1984).

[48] A. Litvinenko, S. Grishin, Y. P. Sharaevskii, V. Tikhonov, and S. Nikitov, A chaotic magnetoacoustic oscillator with delay and bistability, Tech. Phys. Lett. **44**, 263 (2018).

[49] S. E. Sheshukova, E. N. Beginin, A. V. Sadovnikov, Y. P. Sharaevsky, and S. A. Nikitov, Multimode propagation of magnetostatic waves in a width-modulated yttrium-iron-garnet waveguide, IEEE Magn. Lett. **5**, 1 (2014).